AN ALGORITHM FOR MELNIKOV FUNCTIONS AND APPLICATION TO A CHAOTIC ROTOR[*]

JIAN-XIN XU[†], RUI YAN[†], AND WEINIAN ZHANG[‡]

Abstract. In this work we study a dynamical system with a complicated nonlinearity, which describes oscillation of a turbine rotor, and give an algorithm to compute Melnikov functions for analysis of its chaotic behavior. We first derive the rotor model whose nonlinear term brings difficulties to investigating the distribution and qualitative properties of its equilibria. This nonlinear model provides a typical example of a system for which the homoclinic and heteroclinic orbits cannot be analytically determined. In order to apply Melnikov's method to make clear the underlying conditions for chaotic motion, we present a generic algorithm that provides a systematic procedure to compute Melnikov functions numerically. Substantial analysis is done so that the numerical approximation precision at each phase of the computation can be guaranteed. Using the algorithm developed in this paper, it is straightforward to obtain a sufficient condition for chaotic motion under damping and periodic external excitation, whenever the rotor parameters are given.

Key words. mathematical modeling, Melnikov function, chaos, modulus of continuity, oscillatory integrand

AMS subject classifications. 34C28, 34C37, 34C45

DOI. 10.1137/S1064827503420726

1. Introduction. The oscillation phenomenon of the turbine rotor has long been observed in industry. Many efforts [7, 8] have been made to analyze and control the mode and scale of such oscillations, which are caused by a number of factors, e.g., unbalanced centrifugal force. However, to eliminate such vibrations effectively, which are harmful to the quality and life span of the system, it is necessary to examine the underlying nature of those nonlinear oscillations and to find the relationship between the oscillatory behavior and the physical parameters of the real system.

Consider the shaft of a rigid rotor supported symmetrically by four equal bearings at the ends on a low-speed balance platform, as shown in Figure 1. The elasticity in each bearing can be modeled equivalently as a spring. Let L denote the length of the shaft, and let c and K denote the length and stiffness of each relaxed spring, respectively. The following linear model is often used [3, 4, 18, 27]:

$$(1.1) \qquad J_s \frac{d^2\theta}{dt^2} + \frac{KL^2}{2}\theta = 0,$$

where J_s is the principal moment of rotation inertia around the symmetric center S and θ is the angular displacement of the rotor shaft from the balanced horizontal position. This linear model, although widely used in studying the rotor's dynamic behavior, is only a linear approximation near the stable equilibrium $\theta = 0$, and thus is unable to capture the nonlinearly oscillatory characteristics. Such a linear model
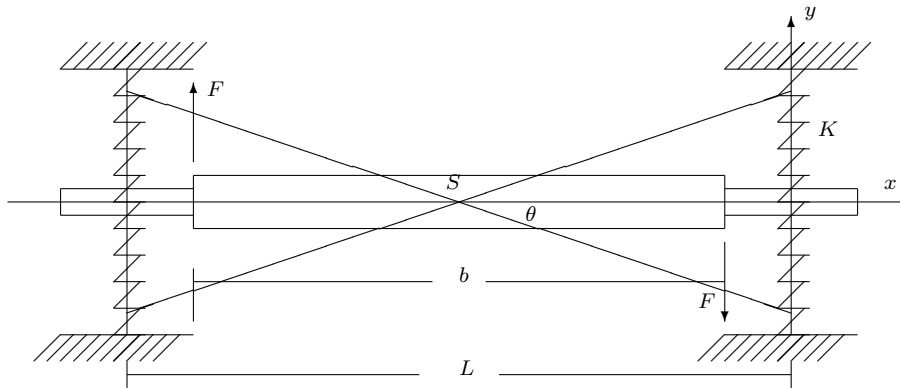
FIG. 1. *Shaft of rotor on a low-speed balance platform.*

fails to explain the observed complex oscillations. Some important nonlinear factors have been neglected in the linear model.

The first objective for this work, therefore, is to establish a nonlinear mathematical model for the rotor system, which turns out to be a class of Hamiltonian systems, with the periodicity coming from the rotational movement of the shaft.

Having established the nonlinear mathematical model, we are concerned with the existence of complex oscillations incurred from system nonlinearities, as done in many works [2, 10, 19, 22, 23, 25]. We are especially interested in the rotor's chaotic motion when it is influenced by damping and periodic external excitation. We look for conditions of the physical parameters that cause transversal intersection of stable manifolds and unstable manifolds, which, according to the dynamical system theory [11], implies chaotic motion. As usual, we need to calculate Melnikov functions along the heteroclinic orbits. Here we encounter two difficult tasks. First, due to the highly complicated nonlinear model, it is too difficult to find analytical expressions for the heteroclinic orbits of the rotor. Second, even if such expressions were given, as in [15, 16, 19], the computation of integrals in Melnikov function would remain a very difficult task. To compute those integrals, the method of residues is applied in [15, 16] and numerical integration with MATLAB software is used in [19].

In applying given methods of bifurcation theory to practical systems, it is of crucial importance to provide appropriate computing algorithms (for instance, see [9, 12, 13]). In particular, without an appropriate algorithm it would be difficult or impossible to apply the Melnikov method to judge homoclinic (or heteroclinic) bifurcations and analyze chaotic motion for many complicated practical models. Recently, increasing interest has been given to the numerical computation of homoclinic and heteroclinic orbits [1, 19, 20]. In [1] numerical approximations of a bifurcation function, which determines periodic solutions of an autonomous differential equation near a homoclinic orbit, are obtained, and a predictor for continuation of the homoclinic orbit is available. In [19] a three-dimensional system modeling chaotic motion of a gyrostat is considered and numerical methods are used to compute Melnikov functions. Nevertheless, there is in general a lack of appropriate algorithms, which can compute Melnikov functions without the closed form of the heteroclinic (homoclinic) orbits. A major purpose of this paper is to present such an algorithm.

In our algorithm many difficulties come from numerical integrals over infinite intervals and numerical integrals of insufficiently smooth integrands or of infinitely
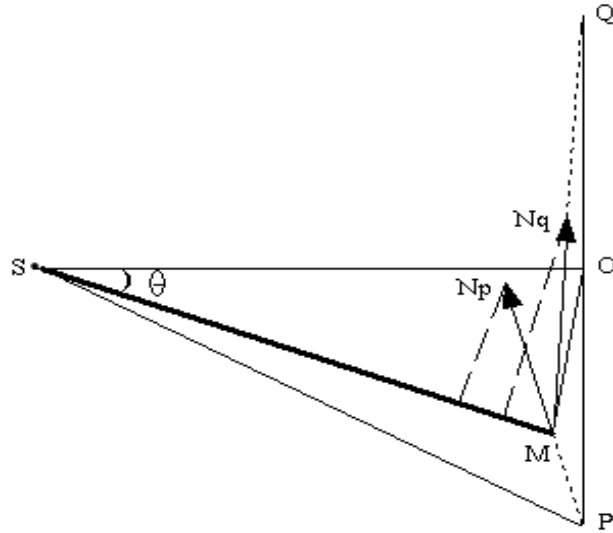
FIG. 2. *Analysis of forces.*

oscillatory integrands. Those difficulties will be overcome by use of such techniques as estimating modulus of continuity and reduction to infinite sums. The effectiveness of our techniques relies on the monotonicity of the heteroclinic orbits, which is related to distribution of equilibria. More precisely, we have to show that there are no other equilibria between the center and the saddle which are linked by the same heteroclinic orbit. Fortunately, this fact is not only exhibited by a numerical simulation but also proved rigorously for concrete L and c by investigating zeros of a polynomial.

This paper is organized as follows. Section 2 gives the nonlinear model. In section 3 we investigate the model for some basic properties, including equilibria and heteroclinic orbits. We show the exact numbers and locations of equilibria under a natural condition. In section 4 we consider the system with damping and periodic external excitation and give an algorithm to compute Melnikov functions. In section 5 we display the conditions for the physical parameters that ensure chaotic motion in the rotor system. With choices of parameters that satisfy the conditions, numerical simulations are implemented to demonstrate our results.

2. Modeling of the nonlinear rotor system. As shown in Figure 2, we analyze the synthesized force exerted on the rotor. Let θ denote the angular displacement of the shaft. The end of the rotor moves from position O to position M. The changes of the lower and upper springs are $|OP| - |MP|$ and $|OQ| - |MQ|$, respectively, where $|OP|$ denotes the length of the vector OP and others are defined in the same manner.

Geometrically,

$$
(2.1) \qquad
\begin{aligned}
|OM|^2 &= |SO|^2 + |SM|^2 - 2|SO| \cdot |SM| \cos\theta \\
&= 2\left(\frac{L}{2}\right)^2 - 2\left(\frac{L}{2}\right)^2 \cos\theta = L^2 \sin^2\frac{\theta}{2}.
\end{aligned}
$$

Obviously, $\angle MOP = \frac{\pi}{2} - (\frac{\pi-\theta}{2}) = \frac{\theta}{2}$ and $\angle MOQ = \frac{\pi}{2} + (\frac{\pi-\theta}{2}) = \pi - \frac{\theta}{2}$. Similarly, we can derive

$$(2.2) \qquad \begin{aligned} |MP|^2 &= |OP|^2 + |OM|^2 - 2|OP| \cdot |OM| \cos \angle MOP \\ &= c^2 + L^2 \sin^2 \frac{\theta}{2} - cL \sin \theta, \end{aligned}$$

$$(2.3) \qquad \begin{aligned} |MQ|^2 &= |OQ|^2 + |OM|^2 - 2|OQ| \cdot |OM| \cos \angle MOQ \\ &= c^2 + L^2 \sin^2 \frac{\theta}{2} + cL \sin \theta, \end{aligned}$$

where $|OP| = |OQ| = c$. Thus we can compute magnitudes of spring forces

$$(2.4) \qquad N_p = K(|OP| - |MP|) = K \left(c - \sqrt{c^2 + L^2 \sin^2 \frac{\theta}{2} - cL \sin \theta} \right),$$

$$(2.5) \qquad N_q = K(|OQ| - |MQ|) = K \left(c - \sqrt{c^2 + L^2 \sin^2 \frac{\theta}{2} + cL \sin \theta} \right).$$

To compute the torque with respect to S, N_p and N_q should be projected to the normal direction of the rotor axis. Define

$$\begin{aligned} \beta_p &:= \angle N_p MS = \angle SMO - \angle N_p MO \\ &= \left(\frac{\pi - \theta}{2} \right) - (\angle MOP + \angle MPO) = \frac{\pi}{2} - \theta - \angle MPO, \\ \beta_q &:= \angle N_q MS = \angle SMO - \angle N_q MO \\ &= \left(\frac{\pi - \theta}{2} \right) - (\pi - \angle MOQ - \angle MQO) = \frac{\pi}{2} - \theta + \angle MQO. \end{aligned}$$

In what follows,

$$\begin{aligned} \sin \beta_p &= \cos(\theta + \angle MPO) = \cos \theta \cos \angle MPO - \sin \theta \sin \angle MPO \\ &= \cos \theta \frac{|OP|^2 + |MP|^2 - |OM|^2}{2 |OP| \cdot |MP|} - \sin \theta \frac{|OM|}{|MP|} \sin \frac{\theta}{2} \\ &= \cos \theta \frac{c^2 + c^2 + L^2 \sin^2 \frac{\theta}{2} - cL \sin \theta - L^2 \sin^2 \frac{\theta}{2}}{2c \sqrt{c^2 + L^2 \sin^2 \frac{\theta}{2} - cL \sin \theta}} \\ &\quad - \frac{L \sin^2 \frac{\theta}{2} \sin \theta}{\sqrt{c^2 + L^2 \sin^2 \frac{\theta}{2} - cL \sin \theta}} \\ &= \frac{-\frac{L}{2} \sin \theta + c \cos \theta}{\sqrt{c^2 + \frac{L^2}{2} - \frac{L^2}{2} \cos \theta - cL \sin \theta}}, \end{aligned}$$

(2.6)

$$\sin \beta_q = \cos(\theta - \angle MQO) = \cos \theta \cos \angle MQO + \sin \theta \sin \angle MQO$$

$$= \cos \theta \frac{|OQ|^2 + |MQ|^2 - |OM|^2}{2 |OQ| \cdot |MQ|} + \sin \theta \frac{|OM|}{|MQ|} \sin \angle MOQ$$

$$(2.7) \qquad = \cos \theta \frac{c^2 + c^2 + L^2 \sin^2 \frac{\theta}{2} + cL \sin \theta - L^2 \sin^2 \frac{\theta}{2}}{2c\sqrt{c^2 + L^2 \sin^2 \frac{\theta}{2} + cL \sin \theta}}$$

$$+ \frac{L \sin^2 \frac{\theta}{2} \sin \theta}{\sqrt{c^2 + L^2 \sin^2 \frac{\theta}{2} + cL \sin \theta}}$$

$$= \frac{\frac{L}{2} \sin \theta + c \cos \theta}{\sqrt{c^2 + \frac{L^2}{2} - \frac{L^2}{2} \cos \theta + cL \sin \theta}}.$$

According to Figure 2, the synthesized torque along the normal direction is $L(-N_p \sin \beta_p + N_q \sin \beta_q)$, where the sign "$-$" comes from the opposite actions of upper spring and lower spring, which are always simultaneously extending and contracting, respectively. Let

$$(2.8) \qquad g(\theta) := L\big(N_p \sin \beta_p - N_q \sin \beta_q\big).$$

As a consequence, the nonlinear mathematical model

$$(2.9) \qquad J_s \frac{d^2\theta}{dt^2} + g(\theta) = 0$$

describes the free oscillations of the rotor shaft.

Further substituting (2.4), (2.5), (2.6), and (2.7) into (2.8) yields

$$g(\theta) = LK \left(c - \sqrt{c^2 + L^2 \sin \frac{\theta}{2} - cL \sin \theta} \right) \frac{-\frac{L}{2} \sin \theta + c \cos \theta}{\sqrt{c^2 + \frac{L^2}{2} - \frac{L^2}{2} \cos \theta - cL \sin \theta}}$$

$$- LK \left(c - \sqrt{c^2 + L^2 \sin \frac{\theta}{2} + cL \sin \theta} \right) \frac{\frac{L}{2} \sin \theta + c \cos \theta}{\sqrt{c^2 + \frac{L^2}{2} - \frac{L^2}{2} \cos \theta + cL \sin \theta}}$$

$$(2.10)$$

$$= -K\sqrt{\Delta} \sin(\theta - \psi) \left(\frac{c}{\sqrt{c^2 + L^2/2 - \sqrt{\Delta} \cos(\theta - \psi)}} - 1 \right)$$

$$- K\sqrt{\Delta} \sin(\theta + \psi) \left(\frac{c}{\sqrt{c^2 + L^2/2 - \sqrt{\Delta} \cos(\theta + \psi)}} - 1 \right),$$

where $\Delta = (L^2/2)^2 + (cL)^2$ and $\psi = \arccos(\frac{L^2/2}{\sqrt{\Delta}})$, and $\psi = \angle OSP$ as shown in Figure 2.

3. Analysis of unperturbed system. For the convenience of computation we take $J_s = 1$. Equation (2.9) is a Hamiltonian system and equivalent to

$$(3.1) \qquad \frac{d\theta}{dt} = \eta, \qquad \frac{d\eta}{dt} = -g(\theta).$$

The energy function is

$$H(\theta, \eta) = \frac{\eta^2}{2} + G(\theta),$$

$$G(\theta) := \int_0^\theta g(\zeta)\, d\zeta$$

$$(3.2) \qquad = 2Kc\left(2c - \sqrt{c^2 + L^2/2 - \sqrt{\Delta}\cos(\theta - \psi)}\right.$$

$$\left. - \sqrt{c^2 + L^2/2 - \sqrt{\Delta}\cos(\theta + \psi)}\right)$$

$$+ K\sqrt{\Delta}(2\cos\psi - \cos(\theta - \psi) - \cos(\theta + \psi)).$$

Here $\frac{\eta^2}{2}$ and $G(\theta)$ represent the kinetic energy and the potential energy, respectively. In practice, L is always much greater than c (simply denoted by $L \gg c$); for example, $L = 4.765\,m$ and $c = 0.00138\,m$.

Investigating all equilibria of system (3.1) is the first step to study its dynamics. It is easy to check that $-\pi$, 0, π are zeros of g in the interval $[-\pi, \pi]$; thus the system has at least three equilibria, $A_- : (-\pi, 0)$, $O : (0, 0)$, and $A_+ : (\pi, 0)$ for $\theta \in [-\pi, \pi]$. However, it is not easy to determine whether the complicated g has other equilibria in the interval $\theta \in [-\pi, \pi]$. Let $s := L/c$ and rewrite g in (2.10) as

$$(3.3) \qquad\qquad g(\theta) = K\sqrt{\Delta}g_0(\theta),$$

where

$$(3.4) \qquad \begin{aligned} g_0(\theta) = {}&- \sin(\theta - \psi)\left(\frac{\sqrt{2}}{\sqrt{2 + 2s^2 - \sqrt{s^4 + 4s^2}\cos(\theta - \psi)}} - 1\right) \\ &- \sin(\theta + \psi)\left(\frac{\sqrt{2}}{\sqrt{2 + 2s^2 - \sqrt{s^4 + 4s^2}\cos(\theta + \psi)}} - 1\right), \end{aligned}$$

and $\psi := \arccos(s/\sqrt{2s^2 + 4})$. Let $g_{\min}$ denote the minimal of $g_0(\theta)$ on $[0, \pi]$. Clearly $g_{\min}$ is a continuous function of the new parameter s. Numerically plotting $g_{\min}(s)$ in Figure 3 shows that when s is approximately greater than 2.0, i.e., $L \gg 2c$, $g(\theta)$ has no other zeros between 0 and π. The same conclusion can also be made on $(-\pi, 0)$ by symmetry.

It is worth mentioning that because of inevitable error, the above numerical simulation may not be able to provide a rigorous proof to prove the existence of zeros of g_0 in a definite interval. The following theorem demonstrates that we can prove rigorously the exclusion of other equilibria for any specified parameters L and c when $L \gg c$.

THEOREM 3.1. *The system (3.1) is 2π-periodic and has equilibria $O : (0, 0)$, $A_- : (-\pi, 0)$, and $A_+ : (\pi, 0)$ for $\theta \in [-\pi, \pi]$. For given $L = 4.765$ and $c = 0.00138$, the system (3.1) has exactly these three equilibria in $[-\pi, \pi]$. Moreover, when $L \gg c$ (for instance, $L = 4.765$ and $c = 0.00138$), O is a center and both A_- and A_+ are saddles. The curve $H(\theta, \eta) = h_*$, where $h_* := 2Kc(2c - 2\sqrt{c^2 + L^2}) + 2KL^2$, has two branches Γ_+ and Γ_-, which are two heteroclinic orbits both connecting A_- and A_+ but which lie in the upper half-plane and lower half-plane, respectively. For each*
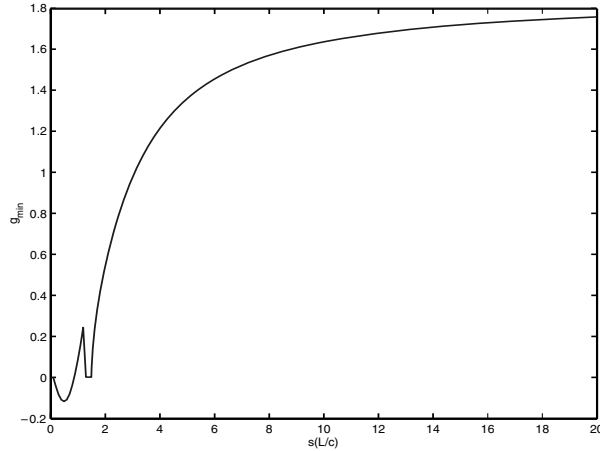
FIG. 3. *Plot the minimal of $g_0(s)$.*

$h \in (0, h_*)$, the curve $H(\theta, \eta) = h$ is a periodic orbit Γ_h around O and surrounded by $\Gamma_\pm$.

Proof. The periodicity of the system is implied by the periodicity of g. Thus it suffices to discuss the system for θ in the interval $[-\pi, \pi]$. It is immediately obvious that the system has at least three equilibria $A_- : (-\pi, 0)$, $O : (0, 0)$, and $A_+ : (\pi, 0)$ for $\theta \in [-\pi, \pi]$. For given $L = 4.765$ and $c = 0.00138$, we further claim that g has no zeros in the open interval $(0, \pi)$.

Consider g_0 as in (3.4). It can be factorized as $g_0(\theta) = -\frac{U(\theta)}{U_+ U_-}$ with $U_\pm = [1 + s^2/2 - \sqrt{s^4/4 + s^2} \cos(\theta \pm \psi)]^{1/2}$ nonsingular and

$$
(3.5) \quad
\begin{aligned}
U(\theta) &= \big[\sin(\theta) \cos(\psi) + \cos(\theta) \sin(\psi) \big] U_- \\
&\quad + \big[\sin(\theta) \cos(\psi) - \cos(\theta) \sin(\psi) \big] U_+ - 2 \sin(\theta) \cos(\psi) U_+ U_- .
\end{aligned}
$$

Clearly, all zeros of g can be calculated from $U(\theta) = 0$. Take a change of variable $z := \cos \theta$, which in fact defines a homeomorphism from $(0, \pi)$ onto $(-1, 1)$. Let $\tilde{U}(z) := U(\arccos z)$. Rationalizing the equality $\tilde{U}(z) = 0$ leads to a polynomial equation

$$
(3.6) \quad (z - 1)(z + 1)P(z) = 0,
$$

where

$$
\begin{aligned}
(3.7) \quad P(z) &:= \big(s^{10} + 8s^8 + 16s^6\big)z^6 + \big(-4s^{10} - 22s^8 - 16s^6 + 32s^4\big)z^5 \\
&\quad + \big(5s^{10} + 10s^8 - 20s^6 + 28s^4 + 32s^2 - 64\big)z^4 \\
&\quad + \big(20s^8 - 120s^4 + 64s^2 + 128\big)z^3 + \big(-5s^{10} - 20s^8 + 40s^6 + 32s^4 - 64s^2\big)z^2 \\
&\quad + \big(4s^{10} + 2s^8 - 16s^6 + 24s^4 - 32s^2\big)z + \big(-s^{10} + 2s^8 - 4s^6 + 4s^4\big)
\end{aligned}
$$

and $s := L/c = 3665.384615$. To find all real roots of $P(z)$, we use the Maple-V7 software command "**realroot** $(P, 1/100{,}000)$," which immediately gives isolating intervals of width $1/100{,}000$ by its internal symbolic operations

$$
\left[\frac{268435411}{268435456}, \frac{67108853}{67108864} \right], \qquad \left[-1, \frac{-131071}{131072} \right],
$$

covering all real roots of $P(z)$. These two intervals in the variable z correspond to the intervals

(3.8) $\qquad [5.789646011 \times 10^{-4}, 5.725382162 \times 10^{-4}], \quad [3.137686400, \pi]$

in θ, respectively.

On the other hand, for $\theta \in (0, \ \psi)$, where $\psi = \arccos(\frac{L^2/2}{\sqrt{\Delta}}) = 5.793099424 \times 10^{-4}$, it can be seen that $\sin(\theta - \psi) < 0$, $\sin(\theta + \psi) > 0$, $\cos(\theta - \psi) > \cos(-\psi) = \frac{L^2/2}{\sqrt{\Delta}}$, and $\cos(\theta + \psi) < \cos(\psi) = \frac{L^2/2}{\sqrt{\Delta}}$. Thus

(3.9) $\quad \sqrt{c^2 + \frac{L^2}{2} - \sqrt{\Delta} \cos(\theta - \psi)} < c, \qquad \sqrt{c^2 + \frac{L^2}{2} - \sqrt{\Delta} \cos(\theta + \psi)} > c.$

Hence in terms of (2.10), $g(\theta) > 0$ on the interval $(0, \psi)$. The first interval in (3.8) is obviously contained in $(0, \psi)$; therefore, the real root of $P(z)$ in the first interval is an additional one arising in the rationalization procedure of $\tilde{U}(z)$. It is actually not a root of g.

To show that the real root of $P(z)$ in the second interval in (3.8) is not a root of g, we notice that the second interval is contained in $(2\psi, \pi]$. Similar to (3.9), for $\theta \in (2\psi, \pi - \psi)$, we have $\sin(\theta - \psi) > 0$, $\sin(\theta + \psi) > 0$, and

$$\sqrt{c^2 + \frac{L^2}{2} - \sqrt{\Delta} \cos(\theta - \psi)} > c, \qquad \sqrt{c^2 + \frac{L^2}{2} - \sqrt{\Delta} \cos(\theta + \psi)} > c.$$

Hence in terms of (2.10), $g(\theta) > 0$ on the interval $(2\psi, \pi - \psi)$. For $\theta \in [\pi - \psi, \pi)$, define

$$g_p(\theta) := -\sqrt{\Delta} \sin(\theta - \psi) \left(\frac{c}{\sqrt{c^2 + L^2/2 - \sqrt{\Delta} \cos(\theta - \psi)}} - 1 \right),$$

$$g_q(\theta) := \sqrt{\Delta} \sin(\theta + \psi) \left(\frac{c}{\sqrt{c^2 + L^2/2 - \sqrt{\Delta} \cos(\theta + \psi)}} - 1 \right).$$

For the given $L = 4.765$ and $c = 0.00138$, note that $\frac{\pi}{2} - \psi \leq \frac{\theta - \psi}{2} < \frac{\pi}{2} - \frac{\psi}{2}$ and $\sin(\theta - \psi) < |\cos(\theta - \psi)| < 1$ for $\theta \in [\pi - \psi, \pi)$. Using Maple-V7 we have

(3.10)
$$\begin{aligned}
\frac{d}{d\theta} g_p(\theta) &= 11.35261440 \cos(\theta - \psi) \left(1 - \frac{0.00138}{\sqrt{22.7052288} \sin(\frac{\theta - \psi}{2})} \right) \\
&\quad + \frac{0.08892847907 \sin^2(\theta - \psi)}{(22.7052288)^{3/2} \sin^3(\frac{\theta - \psi}{2})} \\
&< 11.35261440 \cos(\theta - \psi) \left(1 - \frac{0.00138}{\sqrt{22.7052288} \sin(\frac{\pi}{2} - \psi)} \right) \\
&\quad + \frac{0.08892847907 \sin^2(\theta - \psi)}{(22.7052288)^{3/2} \sin^3(\frac{\pi}{2} - \psi)} \\
&= 11.34932655 \cos(\theta - \psi) + 0.0008219629813 \sin^2(\theta - \psi) \\
&< 0.
\end{aligned}$$

Similarly, noting that $\frac{\pi}{2} \leq \frac{\theta+\psi}{2} < \frac{\pi}{2} + \frac{\psi}{2}$ and $\sin(\theta + \psi) < |\cos(\theta + \psi)| < 1$ for $\theta \in [\pi - \psi, \pi)$, we can derive

$$
\begin{aligned}
\frac{d}{d\theta} g_q(\theta) &= -11.35261440 \cos(\theta + \psi) \left(1 - \frac{0.00138}{\sqrt{22.7052288}\sin(\frac{\theta+\psi}{2})}\right) \\
&\quad - \frac{0.08892847907 \sin^2(\theta + \psi)}{(22.7052288)^{3/2} \sin^3(\frac{\theta+\psi}{2})} \\
&> -11.35261440 \cos(\theta + \psi) \left(1 - \frac{0.00138}{\sqrt{22.7052288}\sin(\frac{\pi}{2} + \frac{\psi}{2})}\right) \\
&\quad - \frac{0.08892847907 \sin^2(\theta + \psi)}{(22.7052288)^{3/2} \sin^3(\frac{\pi}{2} + \frac{\psi}{2})} \\
&= -11.34932655 \cos(\theta + \psi) - 0.0008219626723 \sin^2(\theta + \psi) \\
&> 0.
\end{aligned}
\tag{3.11}
$$

Moreover, it is easy to check that $g_p(\pi - \psi) > g_q(\pi - \psi) = 0$ and $g_p(\pi) = g_q(\pi)$. By (3.10) and (3.11) we see that $g(\theta) = g_p(\theta) - g_q(\theta) > 0$ on $[\pi - \psi, \pi)$. Therefore, $g(\theta) > 0$ on $(2\psi, \pi)$ and thus g has no zeros in the second interval in (3.8) except for the point π.

As above, the claimed fact that g has no zeros in the interval $(0, \pi)$ is proved. We can similarly prove that g has no zeros in $(-\pi, 0)$. It follows that system (3.1) has only three equilibria, O, A_-, and A_+, in $[-\pi, \pi]$.

Now we continue to discuss the qualitative properties of the equilibria and orbits near them. As a basic knowledge in Chapter V of [14], the potential $G(\theta)$ reaches extrema at equilibria, and an equilibrium $(\theta_0, 0)$ is a center (resp., saddle) when $G(\theta_0)$ reaches a minimal (resp., maximal) value. Notice that

$$
G''(0) = \frac{K}{2c^2}\Delta\left[\sin^2(-\psi) + \sin^2\psi\right] = KL^2 > 0;
$$

hence O is a center. Similarly, let us check

$$
\begin{aligned}
G''(\pm\pi) &= -2K\sqrt{\Delta}\left\{-\cos\psi\left(\frac{c}{\sqrt{c^2 + L^2}} - 1\right) - \frac{c}{2}\sqrt{\Delta}\frac{\sin^2\psi}{(c^2+L^2)^{3/2}}\right\} \\
&= -\frac{KL^2 D(L,c)}{(c^2+L^2)^{3/2}[(c^2+L^2)^{3/2} + (cL^2 + 2c^3)]},
\end{aligned}
\tag{3.12}
$$

where $D(L, c) := L^6 + 2L^4c^2 - c^4L^2 - 3c^6$. Clearly, $D(L, c) \to +\infty$ as $L \to +\infty$. Consequently $D(L, c) > 0$ and $G''(\pm\pi) < 0$ when $L \gg c$, in particular when $L = 4.765\,m$ and $c = 0.00138\,m$. That is, both A_- and A_+ are saddles when $L \gg c$. Furthermore, we can verify that $h_* := H(\pm\pi, 0) = G(\pm\pi)$, which is the energy of the system at A_- and A_+, respectively. The orbits $\Gamma_\pm$ connecting A_- and A_+ lie on the curve

$$
H(\theta, \eta) = h_*.
\tag{3.13}
$$

At the center O we have $H(0, 0) = G(0) = 0$. Therefore, each $h \in (0, h_*)$ determines a closed curve $H(\theta, \eta) = h$, which is a periodic orbit around O.   □

Remark 1. For any given real system parameters L and c with $L \gg c$, we can derive the same result as given in Theorem 3.1 by following the same procedure as
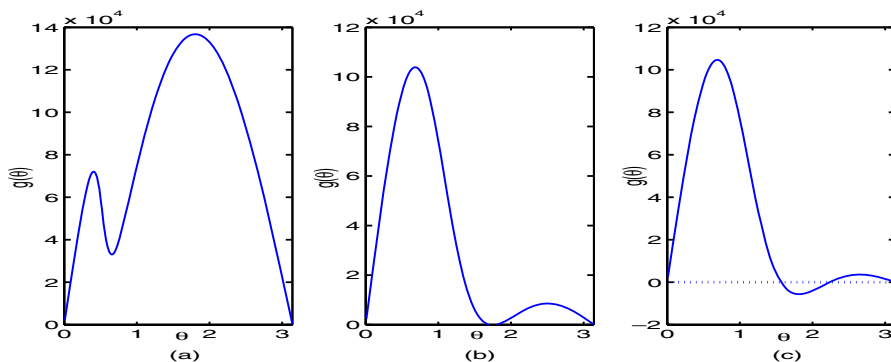
FIG. 4. $g(\theta)$ for (a) $c = 1.38$, (b) $c = 4.0$, (c) $c = 4.2$.

for $L = 4.765$ and $c = 0.00138$. Numerical simulations of g with fixed $L = 4.765$ and $K = 10,000$ but different c, as shown in Figure 4, exhibit the bifurcation of zeros of g in $[-\pi, \pi]$ as c varies around $c_0 \approx 4.0$.

From (3.1) and (3.13) we can see that the heteroclinic solution $\theta_+(t)$ satisfies

$$(3.14) \qquad \dot{\theta} = \sqrt{2(h_* - G(\theta))}.$$

Obviously, $\theta_+(t)$ is the inverse of the function

$$(3.15) \qquad t = \tau(\theta) := \int_0^\theta \frac{d\theta_1}{\sqrt{2(h_* - G(\theta_1))}}, \quad \theta \in (-\infty, +\infty).$$

Since G in (3.2) is an even function, $\tau(\theta)$ and its inverse $\theta_+(t)$ are odd functions. From (3.14), $\eta_+(t) = \dot{\theta}_+(t)$ is an even function.

4. Algorithm for Melnikov functions. Consider system (2.9) with damping and periodic external excitation, that is,

$$(4.1) \qquad J_s \frac{d^2\theta}{dt^2} + g(\theta) = -\Xi \frac{d\theta}{dt} + \Lambda \cos(\omega t),$$

where $g(\theta)$ is given in (2.10), $\Xi > 0$ is the fiction rate, $\Lambda > 0$ is the maximal excitation torque, and ω is the frequency of excitation. In this section we discuss the effect of small damping and small amplitude to system oscillations, and we give regions of parameters where the oscillation is chaotic. For convenience, let $\Xi = \mu\xi$ and $\Lambda = \mu\lambda$, where μ, ξ, λ are all real numbers and $\mu > 0$ is small.

As shown in [11], Smale and Birkhoff proved that transversal intersection of a stable manifold and an unstable manifold causes chaos in the type of horseshoe. For unperturbed system (2.9), the heteroclinic orbits $\Gamma_\pm$, given in Theorem 3.1, are both intersection of the stable manifold of a hyperbolic equilibrium and the unstable manifold of another hyperbolic equilibrium. For system (4.1), by Theorem 4.5.3 in [11], the intersection of stable manifolds and unstable manifolds depends on zeros of Melnikov functions

$$(4.2) \qquad M_\pm(t_0) = \int_{-\infty}^{+\infty} \eta_\pm(t)[-\xi\eta_\pm(t) + \lambda\cos(\omega(t + t_0))]\, dt,$$

where the curves of $\Gamma_\pm$ are denoted by $\theta = \theta_\pm(t)$, $\eta = \eta_\pm(t)$, which are solutions of (3.1). If $M_\pm(t_0)$ has a simple zero, i.e.,

$$M_\pm(t_0) = 0, \qquad M'_\pm(t_0) \neq 0,$$

then the manifolds intersect transversally. If $M_\pm(t_0)$ remains away from zero, then the manifolds do not intersect. Here those invariant manifolds are considered for the Poincaré mapping of the time-periodic system (4.1).

Since $\eta_\pm(t)$ are even functions, from (4.2) we have

(4.3) $$M_\pm(t_0) = -\xi V_\pm + \lambda \cos(\omega t_0) I_\pm,$$

(4.4) $$V_\pm = \int_{-\infty}^{+\infty} \eta_\pm^2(t)\, dt, \qquad I_\pm = \int_{-\infty}^{+\infty} \eta_\pm(t) \cos(\omega t)\, dt.$$

The ratio of $V_\pm$ and $I_\pm$ decides the region of parameters where chaos occurs. More concretely, the region for chaos is described by the inequalities

(4.5) $$\left| \frac{\lambda}{\xi} \right| > R_\pm := \left| \frac{V_\pm}{I_\pm} \right|.$$

Usually, $V_\pm$ and $I_\pm$ are calculated directly with analytic expressions of $\theta_\pm(t)$ and $\eta_\pm(t)$; see, for instance, [11, 15]. In particular, the integral $I_\pm$ can be computed by the method of residues (see p. 191 of [11]), i.e., extending the integrand to a function in complex plane, integrating the function along an appropriately selected path, and computing the residues of singular points surrounded by the path, as shown in detail in [15, 26]. However, that method applies only to Hamiltonian systems in simple forms, with the curves of homoclinic orbits and heteroclinic orbits available analytically. In our case that method does not work because it is difficult to solve $\theta_\pm(t)$ and $\eta_\pm(t)$ in analytical forms for the heteroclinic orbits $\Gamma_\pm$, aside from the technical difficulties in the method of residues.

In the following, we give an algorithm to compute Melnikov functions for the complicated nonlinear system (4.1) where $L \gg c$ (for instance, $L = 4.765$ and $c = 0.00138$) such that g has no zeros in the interval $(0, \pi)$ and the unperturbed system (3.1) has exactly three equilibria O, A_-, and A_+ in $[-\pi, \pi]$, as shown in Theorem 3.1. This algorithm includes computations of the integrals $V_\pm$ and $I_\pm$.

4.1. Computation of $V_\pm$. We illustrate only with V_+. The integrand of V_+ includes the function η_+, which cannot be expressed in the closed form because of the complicated g. Our strategy is to reduce the integral over an infinite interval to an integral over a finite one or reduce the integrand to a simpler one. By the parity of $\theta_+(t)$ and $\eta_+(t)$, and the relation (3.14),

(4.6)
$$V_+ = \int_{-\infty}^{+\infty} \eta_+^2(t)\, dt = 2 \int_0^{+\infty} \eta_+^2(t)\, dt$$
$$= 2 \int_0^\pi \sqrt{2(h_* - G(\theta))}\, d\theta,$$

where the resulting integral includes neither the function $\theta_+(t)$ nor $\eta_+(t)$ in its integrand. Obviously, here our objective is to solve (4.6) numerically.

Although many numerical integration rules (for example, the compound Simpson's rule [5]) can be applied to (4.6), the main difficulty is how to estimate and control

the approximation precision to any desired level. Denote $F(\theta) := \sqrt{2(h_* - G(\theta))}$ and let $V_+(n)$ denote the integral approximation. As for the Simpson's rule, the approximation error

$$(4.7) \qquad\qquad E_V(n) := V_+ - V_+(n)$$

is often estimated by the formula $E_V(n) = -\frac{n\rho^5}{90}F^{(4)}(\zeta)$, where $0 < \zeta < \pi$ and ρ is the length of subdivision of $[0, \pi]$. It requires the fourth order derivative of F on $[0, \pi]$. Unfortunately, by virtue of the complexity in g and G, evaluation of derivatives of F is very difficult, which can be observed from the second order derivative of F,

$$(4.8) \qquad\qquad F''(\theta) = -\frac{g'(\theta)(2(h_* - G(\theta))) + g^2(\theta)}{(\sqrt{2(h_* - G(\theta))})^3}.$$

When $\theta \to \pi$, its limit is in the $\frac{0}{0}$-type and remains in $\frac{0}{0}$-type no matter how many times we differentiate the numerator and denominator simultaneously. Thus the limit cannot be calculated by l'Hôpital's rule. $F^{(3)}$ and $F^{(4)}$ will be even more complicated.

Here we adopt an effective estimation method which, given in section 4.8 of [5], is specifically suitable for a high-order approximation rule to be applied to a low-order continuity function. Define the *modulus of continuity* of a continuous function $f(x)$ on $[a, b]$ by

$$(4.9) \qquad\qquad m_f(\delta) := \max_{|x_1 - x_2| \leq \delta} |f(x_1) - f(x_2)|, \quad a \leq x_1, x_2 \leq b.$$

The following useful result can be found in [5] and [17].

LEMMA 4.1. *Let f and $m_f(\delta)$ be given as above. For each integer $n \geq 1$, there exists a polynomial $p_n(x)$ of degree $\leq n$ such that $|f(x) - p_n(x)| \leq 6m_f(\frac{b-a}{2n})$, $a \leq x \leq b$.*

Now we are in a position to apply the Gauss–Legendre integration rule and deduce the error estimate. With the change of variables $\theta = \frac{\pi}{2}(\vartheta + 1)$, which transforms the interval $[0, \pi]$ into the standard interval $[-1, 1]$ for the Gauss–Legendre rule, we see that

$$V_+ = \pi \int_{-1}^{1} F\left(\frac{\pi}{2}(\vartheta + 1)\right) d\vartheta.$$

Fix an integer $n \geq 1$, and let ϑ_j $(j = 0, 1, \ldots, n)$ be the $n+1$ real zeros of the Legendre polynomial

$$P_{n+1}(x) = \frac{1}{2^n n!} \frac{d^n}{dx^n}\{(x^2 - 1)^n\}.$$

Consider the $(n + 1)$-point Gauss–Legendre rule [5]

$$(4.10) \qquad\qquad \int_{-1}^{1} \varphi(\vartheta)\, \vartheta \approx \mathcal{G}(\varphi, n + 1) = \sum_{j=0}^{n} A_j \varphi(\vartheta_j),$$

where the reals A_j are solved from the system of linear equations given by the exact (4.10) for $\varphi(\vartheta) = 1, \vartheta, \vartheta^2, \ldots, \vartheta^n$. Then we obtain

$$(4.11) \qquad V_+(n) = \pi\mathcal{G}\left(F\left(\frac{\pi}{2}(\vartheta + 1)\right), n + 1\right) = \pi\sum_{j=0}^{n} A_j F\left(\frac{\pi}{2}(\vartheta_j + 1)\right).$$

THEOREM 4.2. *For integer $n \geq 1$, $|E_V(n)| \leq \frac{9\pi^2}{2n} \sup_{0 \leq \theta \leq \pi} |F'(\theta)|$.*

Proof. Let $m_F(\delta)$ denote the modulus of continuity of F. By Lemma 4.1, there exists a polynomial $p_{2n}(\theta)$ of degree $\leq 2n$ such that

$$(4.12) \qquad |F(\theta) - p_{2n}(\theta)| \leq 6 m_F\left(\frac{\pi}{4n}\right)$$

for all $\theta \in [0, \pi]$.

Observe that

$$F'(\theta) = -\frac{g(\theta)}{\sqrt{2(h_* - G(\theta))}} = -\frac{g(\theta)}{F(\theta)},$$

which is continuous on $[0, \pi]$. Moreover, the limit from left $\lim_{\theta \to \pi - 0} F'(\theta)$ exists because $\eta = F(\theta)$ describes the curve of heteroclinic orbit Γ_+ which, being the stable manifold of the saddle $A_+ : (\pi, 0)$ by Theorem 3.1, has a definite tangency at the saddle. By l'Hôpital's rule, the limit $\ell := \lim_{\theta \to \pi - 0} F'(\theta)$ satisfies $\ell = -\lim_{\theta \to \pi - 0} g'(\theta)/\ell$, i.e., $\ell^2 = -G''(\pi) > 0$ by (3.12). Notice that $g(0) = g(\pi) = 0$, and from Theorem 3.1, there are no zeros of $g(\theta)$ in the interval $(0, \pi)$. Thus $g(\theta)$ must be either above or below 0 for all $\theta \in (0, \pi)$. On the other hand, it is easy to verify that $g'(0) > 0$, hence

$$(4.13) \qquad g(\theta) > 0 \quad \forall \theta \in (0, \pi),$$

and therefore $F'(\theta) < 0$ for $\theta \in (0, \pi)$ in terms of (4.8) (or, say, F is decreasing on the interval $(0, \pi)$). Thus $\ell = -\sqrt{-G''(\pi)}$. Consequently, F' is bounded on $[0, \pi]$. Let M_1 be such a bound, i.e.,

$$(4.14) \qquad |F'(\theta)| \leq M_1 \quad \forall \theta \in [0, \pi].$$

Then

$$(4.15) \qquad m_F\left(\frac{\pi}{4n}\right) \leq \frac{\pi M_1}{4n}$$

by the definition (4.9) of modulus of continuity.

It is known (theorem on p. 97 of [5]) that the $(n+1)$-point Gauss–Legendre rule is exact for polynomials of degree $\leq 2n + 1$. Then

$$\int_0^\pi p_{2n}(\theta)\, d\theta = \frac{\pi}{2} \int_{-1}^1 p_{2n}\left(\frac{\pi}{2}(\vartheta + 1)\right) d\vartheta = \frac{\pi}{2} \mathcal{G}\left(p_{2n}\left(\frac{\pi}{2}(\vartheta + 1)\right), n + 1\right).$$

The direct estimation gives

$$\begin{aligned}
|E_V(n)| &= |V_+ - V_+(n)| \\
&= \left| 2 \int_0^\pi (F(\theta) - p_{2n}(\theta))d\theta + 2 \int_0^\pi p_{2n}(\theta)d\theta - \pi \mathcal{G}\left(F\left(\frac{\pi}{2}(\vartheta + 1)\right), n + 1\right) \right| \\
&\leq 2 \int_0^\pi |F(\theta) - p_{2n}(\theta)|\, d\theta + \pi \left| \mathcal{G}\left(p_{2n}\left(\frac{\pi}{2}(\vartheta + 1)\right), n + 1\right) \right. \\
&\qquad\qquad\qquad\qquad\qquad \left. - \mathcal{G}\left(F\left(\frac{\pi}{2}(\vartheta + 1)\right), n + 1\right) \right|.
\end{aligned}$$

Since all weights A_j in (4.10) are positive and satisfy that $\sum_{j=0}^{n} A_j = 1$, we see that

$$\left| \mathcal{G}\left(p_{2n}\left(\frac{\pi}{2}(\vartheta + 1) \right), n+1 \right) - \mathcal{G}\left(F\left(\frac{\pi}{2}(\vartheta + 1) \right), n+1 \right) \right|$$

$$\leq \sum_{j=0}^{n} A_j \left| p_{2n}\left(\frac{\pi}{2}(\vartheta_j + 1) \right) - F\left(\frac{\pi}{2}(\vartheta_j + 1) \right) \right|$$

$$\leq 6 m_F\left(\frac{\pi}{4n} \right) \left(\sum_{j=0}^{n} A_j \right) \leq \frac{3\pi}{2n} M_1$$

by (4.12) and (4.15). By the same reasons we also see that

$$\int_0^{\pi} |F(\theta) - p_{2n}(\theta)| \, d\theta \leq \frac{3\pi^2}{2n} M_1.$$

It follows that

$$|E_V(n)| \leq 2 \frac{3\pi^2}{2n} M_1 + \pi \frac{3\pi}{2n} M_1 = \frac{9\pi^2}{2n} M_1,$$

and this completes the proof. □

Since $F'(\theta)$ is known and bounded, one can give the bound by comparing values at extreme points and endpoints. Consider $K = 10{,}000$, $c = 0.00138$, and $L = 4.765$, for example. The numerator of F'' is

$$\Upsilon(\theta) := -5.155272416 \times 10^{10} \cos^2 \theta - 1.031054484 \times 10^{11} \cos \theta - 5.155272420 \times 10^{10}.$$

Let $z = \cos \theta$. Then

$$\Upsilon(\arccos(z)) = -5.155272416 \times 10^{10} z^2 - 1.031054484 \times 10^{11} z - 5.155272420 \times 10^{10},$$

which has two real zeros at $z = -1.000027856$ and $z = -0.9999721457$. The numerical result suggests that $\arccos(-0.9999721457)$ is the unique possible extreme point of F' in $(0, \pi)$. This implies that

$$|F'(\theta)| \leq \max\{|F'(0)|, |F'(\arccos(-0.9999721457))|, |F'(\pi)|\}$$
$$= \max\{0, 476.4922088, \sqrt{-G''(\pi)}\} = 476.5.$$

We can simply choose $M_1 = 480$. Thus, for a desired error level $\varepsilon > 0$, we can determine by Theorem 4.2 an integer $n > 0$ such that $E_V(n) < \varepsilon$, and in what follows obtain an approximation $V_+(n)$ to meet the precision $\varepsilon > 0$.

4.2. Computation of $I_\pm$. By the parity of η_+,

$$(4.16) \qquad I_+ = \int_{-\infty}^{+\infty} \eta_+(t) \cos(\omega t) \, dt = 2 \int_0^{+\infty} \eta_+(t) \cos(\omega t) \, dt.$$

Clearly the integrand of (4.16) is infinitely oscillatory. Our strategy is to take a truncation of the integration range and treat the integral as a finite one, as in [5] and [24].

Subdividing the integration interval, we can write the integral over an infinite interval as an infinite sum of partial integrals over finite intervals, that is,

$$(4.17) \qquad \int_0^{+\infty} \eta_+(t) \cos(\omega t) \, dt = \sum_{j=0}^{\infty} r_j,$$

where

$$(4.18) \qquad r_j = \int_{t_j}^{t_{j+1}} \eta_+(t) \cos(\omega t)\, dt, \quad j = 1, 2, \ldots,$$

and

$$(4.19) \qquad r_0 = \int_0^{t_1} \eta_+(t) \cos(\omega t)\, dt.$$

The choice of the partition points is arbitrary as long as the sequence of partial integrals r_j is alternating. The most common and simplest way is to select the zeros of the integrand as the partition points, i.e.,

$$t_j = \frac{2k\pi + (2j-3)\pi/2}{\omega}, \quad j = 1, 2, \ldots,$$

where the natural number k was given earlier. Thus

$$r_j = \int_{\frac{2k\pi + (2j-3)\pi/2}{\omega}}^{\frac{2k\pi + (2j-1)\pi/2}{\omega}} \eta_+(t) \cos(\omega t)\, dt, \quad j = 1, 2, \ldots.$$

It follows that $r_{2j-1} > 0$ and $r_{2j} < 0$ $(j = 1, 2, \ldots)$, because $\eta_+(t) > 0$ for $t \in (0, +\infty)$. Furthermore, from the inequality (4.13), implied by Theorem 3.1, we have

$$\dot{\eta}_+(t) = \ddot{\theta}_+(t) = -g(\theta_+(t)) < 0 \quad \forall t \in (0, +\infty),$$

because $0 < \theta_+(t) < \pi$. As a result, $\eta_+(t)$ is a decreasing function and

$$|r_1| > |r_2| > \cdots > |r_j| > \cdots \to 0 \quad \text{as } j \to \infty.$$

Hence the residue of approximation $R(k) := \int_{t_1}^{+\infty} \eta_+(t) \cos(\omega t)\, dt$ satisfies

$$R(k) = \sum_{j=1}^{\infty} (r_{2j-1} + r_{2j}) > 0.$$

On the other hand, we also have $r_{2j} + r_{2j+1} < 0$ for all $j = 1, 2, \ldots$, and

$$R(k) = r_1 + \sum_{j=1}^{\infty} (r_{2j} + r_{2j+1}) \le r_1$$

$$(4.20) \qquad \le \int_{t_1}^{t_2} \eta_+(t)\, dt = \theta_+(t_2) - \theta_+(t_1)$$

$$= \theta_+\left(\frac{2k\pi + \pi/2}{\omega}\right) - \theta_+\left(\frac{2k\pi - \pi/2}{\omega}\right).$$

Note that both t_1 and t_2 are functions of k and tend to $+\infty$ as $k \to \infty$. Therefore, both $\theta_+(t_1)$ and $\theta_+(t_2)$ tend to π, and $R(k) \to 0$, as $k \to \infty$.

For a given error $\varepsilon > 0$, our computation for I_+ is implemented as follows.

Step 1. Determine the value of k for a truncation error $R(k) \le \varepsilon/4$.

Observe that $t_2 - t_1 = \frac{\pi}{\omega}$. Take the sequence $\{\tau_i\}$ of equally spaced points with pace $\rho = \frac{\pi}{2m\omega}$ as a partition of $[0, t_2]$, where m is a positive integer. Clearly both t_1 and t_2 are included in the sequence. Apply Euler's method to (3.14), i.e.,

$$\theta_{+,m}(\tau_{i+1}) = \theta_{+,m}(\tau_i) + \rho\sqrt{2[h_* - G(\theta_{+,m}(\tau_i))]},$$

$$\tilde{\theta}_{+,m}(\tau_{i+1}) := \theta_+(\tau_{i+1}) - \theta_{+,m}(\tau_{i+1}) \approx \frac{\rho^2}{2}\ddot{\theta}_+(\tau_i) = -\frac{\rho^2}{2}g(\theta_+(\tau_i)),$$

to compute $\theta_+(t_1)$ and $\theta_+(t_2)$ as required in (4.20). For a given k, first take a sufficiently large $m > 0$ (i.e., a sufficiently small ρ) such that $|\tilde{\theta}_{+,m}(t_1)| \leq \frac{\varepsilon}{16}$ and $|\tilde{\theta}_{+,m}(t_2)| \leq \frac{\varepsilon}{16}$. This means that $\theta_{+,m}(t_j)$ can be used to approximate the unknown $\theta_+(t_j)$ in estimating $R(k)$, $j = 1, 2$. If the inequality

$$(4.21) \qquad \qquad \theta_{+,m}(t_2) - \theta_{+,m}(t_1) \leq \frac{\varepsilon}{8}$$

is not satisfied, then repeat the same procedure for $k + 1$. By the convergence of $R(k)$ as $k \to \infty$, indicated just after (4.20), there exists a finite k such that $R(k) \leq \varepsilon/4$.

Step 2. Compute the finite integration $r_0 = \int_0^{t_1} \eta_+(t)\cos(\omega t)\,dt$.

After determining the integer k in Step 1, the value of t_1 is fixed. Integrating by parts we obtain

$$
\begin{aligned}
(4.22) \qquad r_0 &= \int_0^{t_1} \cos(\omega t)\, d\,\theta_+(t) \\
&= \theta_+(t)\cos(\omega t)\big|_0^{t_1} + \omega \int_0^{t_1} \theta_+(t)\sin(\omega t)\,dt \\
&= \omega \int_0^{t_1} \theta_+(t)\sin(\omega t)\,dt.
\end{aligned}
$$

Let $s_i = i\rho$ for $i = 0, 1, \ldots, 2n$, where $\rho = \frac{t_1}{2n} = \frac{2k\pi - \pi/2}{2n\omega}$. $\{s_0, \ldots, s_{2n}\}$ is a sequence of equally spaced points in $[0, t_1]$ with $s_{i+1} - s_i = \rho$ for each i. Applying Simpson's rule we have

$$
\begin{aligned}
(4.23) \qquad r_0 &= \frac{\omega\rho}{3}\Bigg[\theta_+(0)\sin(0) + 4\sum_{i=1}^{n}\theta_+(s_{2i-1})\sin(\omega s_{2i-1}) \\
&\qquad + 2\sum_{i=1}^{n-1}\theta_+(s_{2i})\sin(\omega s_{2i}) + \theta_+(t_1)\sin(\omega t_1)\Bigg] + E_1(n),
\end{aligned}
$$

where the approximation error of Simpson's rule is

$$(4.24) \quad E_1(n) = -\frac{\omega\rho^4}{180}[\Theta^{(3)}(t_1) - \Theta^{(3)}(0)], \qquad \Theta^{(3)}(t) := \frac{\partial^3(\theta_+(t)\sin(\omega t))}{\partial t^3}.$$

To compute $\theta_+(s_{2i-1}), \theta_+(s_{2i})$, and $\theta_+(t_1)$, we use Euler's rule as shown in Step 1 and use the same partition adopted in Simpson's rule. Thus

$$r_0 - E_1(n) = \frac{\omega\rho}{3}\Biggl\{4\sum_{i=1}^{n}\theta_+(s_{2i-1})\sin(\omega s_{2i-1})$$

$$+ 2\sum_{i=1}^{n-1}\theta_+(s_{2i})\sin(\omega s_{2i}) + \theta_+(t_1)\sin(\omega t_1)\Biggr\}$$

$$= \frac{\omega\rho}{3}\Biggl\{4\sum_{i=1}^{n}\bigl[\theta_{+,n}(s_{2i-1}) + \tilde{\theta}_{+,n}(s_{2i-1})\bigr]\sin(\omega s_{2i-1})$$

$$+ 2\sum_{i=1}^{n-1}\bigl[\theta_{+,n}(s_{2i}) + \tilde{\theta}_{+,n}(s_{2i})\bigr]\sin(\omega s_{2i})$$

$$+ \bigl[\theta_+(t_1) + \tilde{\theta}_{+,n}(t_1)\bigr]\sin(\omega t_1)\Biggr\}$$

$$= I_+(n) + E_2(n),$$

where

$$(4.25)\qquad I_+(n) := \frac{\omega\rho}{3}\Biggl[4\sum_{i=1}^{n}\theta_{+,n}(s_{2i-1})\sin(\omega s_{2i-1})$$

$$+ 2\sum_{i=1}^{n-1}\theta_{+,n}(s_{2i})\sin(\omega s_{2i}) + \theta_{+,n}(t_1)\sin\omega t_1\Biggr],$$

$$(4.26)\qquad E_2(n) := \frac{\omega\rho}{3}\Biggl[4\sum_{i=1}^{n}\tilde{\theta}_{+n}(s_{2i-1})\sin(\omega s_{2i-1})$$

$$+ 2\sum_{i=1}^{n-1}\tilde{\theta}_{+n}(s_{2i})\sin(\omega s_{2i}) + \tilde{\theta}_{+n}(t_1)\sin\omega t_1\Biggr].$$

Note that $I_+(n)$, $E_1(n)$, and $E_2(n)$ depend on the choice of k, because s_j and t_1 depend on the choice of k. Let us use the notations $I_+(n,k)$, $E_1(n,k)$, and $E_2(n,k)$ as explicit functions of k. Then the integration is

$$I_+ = 2I_+(n,k) + E_I(n,k),$$

where

$$(4.27)\qquad E_I(n,k) := 2[E_1(n,k) + E_2(n,k)] + 2R(k).$$

Having computed $\theta_+(0)$ and $\theta_+(t_1)$ as above, we can compute derivatives of $\theta_+(t)$ up to third order at 0 and t_1, for instance, at t_1, by

$$\dot{\theta}_+(t_1) = \sqrt{2[h_* - G(\theta_{+,n}(t_1))]},$$

$$\ddot{\theta}_+(t_1) = -g(\theta_{+,n}(t_1)),$$

$$\theta_+^{(3)}(t_1) = -\frac{dg}{d\theta}(\theta_{+,n}(t_1))\sqrt{2[h_* - G(\theta_{+,n}(t_1))]},$$

so that $\Theta^{(3)}(0)$ and $\Theta^{(3)}(t_1)$ in (4.24) and therefore the approximation error $E_1(n,k)$ can be estimated. By the convergence of Euler's and Simpson's rules, we can choose a sufficiently large integer n, such that $|E_1(n,k) + E_2(n,k)| < \varepsilon/4$.

Both n and k having been determined, the approximation $2I_+(n, k)$ of I_+ is computed by (4.25) and, by (4.27), the approximation error $E_I(n, k)$ for I_+ is guaranteed less than ε.

Remark 2. In solving the differential equation (3.14), we adopt the elementary Euler rule to show our ideas of computation clearly. We can also use the Runge–Kutta rule.

Remark 3. As shown in [6] and [21], in Step 1 we can also let the partition points t_j be the extrema of $\cos(\omega t)$ to get a faster convergence of the sequence of partial sums $\sum_{j=0}^{\infty} r_j$.

5. Chaotic oscillation. In the previous section we obtained the approximations $V_+(n)$ and $2I_+(n, k)$ of the integrals V_+ and I_+ for any given precision $\varepsilon > 0$. By symmetry we know that $V_+ = V_-$ and $I_+ = -I_-$. In terms of Theorem 4.5.3 in [11], for sufficiently small $\mu > 0$ and for ξ and $\lambda > 0$ satisfying (4.5), system (4.1) has chaos of the horseshoe type. Based on the previous relation between Ξ, Λ and ξ, λ, we finally reach the following conclusion.

THEOREM 5.1. *For arbitrary small $\varepsilon > 0$ there exist positive integers k, n, and n' such that system* (4.1) *has chaos of horseshoe type in the region*

$$\mathcal{K}_\varepsilon^1 = \left\{ (\Xi, \Lambda) \in \mathbf{R}^2 : \left| \frac{\Lambda}{\Xi} \right| > \frac{V_+(n) + \varepsilon}{2I_+(n', k) - \varepsilon} \right\}.$$

This result is given with absolute error. Sometimes computation with relative error may be more efficient. For example, with the parameter values: $L = 4.765\, m$, $c = 0.00138\, m$, $K = 10000\, N/m$, $J_s = 1$, and $\omega = 1.8\, \pi$, we have to take $n = 1,065,950$ in (4.11) by Theorem 4.2 even if we only hope an absolute error $\varepsilon = 0.02$. Our Pentium IV computer cannot process such a 1,065,950-point Gauss–Legendre rule. However, only for $n = 250$ we obtain $E_V(n)/V_+(n) \approx 0.0186$, which satisfies the relative error $\varepsilon' = 0.02$. In this case, $V_+(n) = 3769.3144$ and $E_V(n) = 70.1092$. Inspired by the idea, we obtain some analogies of Theorem 5.1.

COROLLARY 5.2. *For arbitrary small $\varepsilon > 0$ and $\varepsilon' > 0$ there exist positive integers k, n, and n' such that system* (4.1) *has chaos of horseshoe type in the region*

$$\mathcal{K}_{\varepsilon, \varepsilon'}^2 = \left\{ (\Xi, \Lambda) \in \mathbf{R}^2 : \left| \frac{\Lambda}{\Xi} \right| > \frac{(1 + \varepsilon')V_+(n)}{2I_+(n', k) - \varepsilon} \right\}.$$

COROLLARY 5.3. *For arbitrary small $\varepsilon' > 0$ there exist positive integers k, n, and n' such that system* (4.1) *has chaos of horseshoe type in the region*

$$\mathcal{K}_{\varepsilon'}^3 = \left\{ (\Xi, \Lambda) \in \mathbf{R}^2 : \left| \frac{\Lambda}{\Xi} \right| > \frac{(1 + \varepsilon')V_+(n)}{2(1 - \varepsilon')I_+(n', k)} \right\}.$$

Actually, in Corollary 5.2, $E_V(n) \leq \varepsilon' V_+(n)$, where $\varepsilon' > 0$ is the desired relative error. Then $V_+ \leq V_+(n) + E_V(n) \leq (1 + \varepsilon')V_+(n)$. Corollary 5.3 is explained similarly.

Apply Corollary 5.2 to system (4.1) with L, c, K, J_s, and ω chosen above. Taking $\varepsilon = 0.001$ and $\varepsilon' = 0.02$, we get $n = 250$, $n' = 60,000$, $k = 10$ and correspondingly obtain $V_+(n) = 3769.3144$ and $I_+(n, k) = 11.4177$. Numerical computation gives that $\mathcal{K}_{\varepsilon, \varepsilon'}^2 = \{ (\Xi, \Lambda) \in \mathbf{R}^2 : |\frac{\Lambda}{\Xi}| > 336.7611 \}$. Similarly, for the same values $L = 4.765$, $c = 0.00138$, $J_s = 1$, and $\omega = 1.8\pi$ but the smaller $K = 10$, by Corollary 5.2 we get $\mathcal{K}_{\varepsilon, \varepsilon'}^2 = \{ (\Xi, \Lambda) \in \mathbf{R}^2 : |\frac{\Lambda}{\Xi}| > 1.9449 \}$.

Numerical simulation for trajectories of system (4.1) can hardly display convincing evidence for chaotic behavior because the system is nonautonomous. Theoretically,
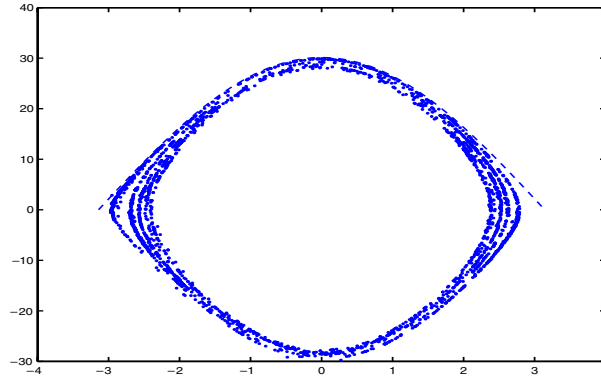
FIG. 5. $\Xi = 0.02$ and $\Lambda = 0$.
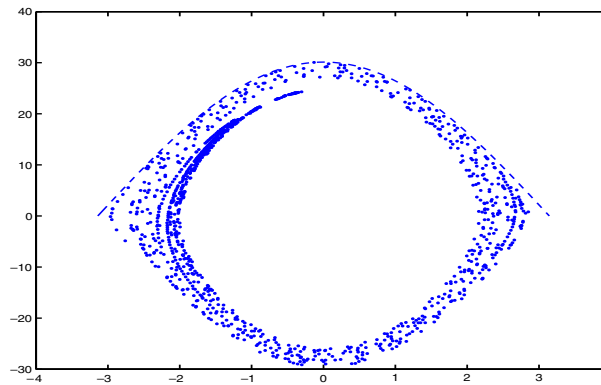
FIG. 6. $\Xi = 0.02$ and $\Lambda = 0.005$.

iteration of its Poincaré map on the stable manifold and the unstable manifold can describe chaos well. However, it is not easy to simulate the two invariant manifolds on a Poincaré section. Here we use the simulation method in [11], where the partial plots of the invariant manifolds are produced by iterating a number of points defining a short segment of the manifolds near the saddle under the Poincaré map (or its inverse). Actually, the Poincaré map is structurally stable near saddles, so it is near the invariant set of horseshoe. By continuous dependence, the simulation of orbits under the Poincaré map near the pair of invariant manifolds can also reflect chaotic behavior.

In our case the Poincaré map is

$$\Pi : (\theta_0, \eta_0) \mapsto (\theta(2\pi/\omega, \theta_0, \eta_0), \eta(2\pi/\omega, \theta_0, \eta_0)),$$

where $\eta(t, \theta_0, \eta_0) = \dot{\theta}(t, \theta_0, \eta_0)$ and $(\theta(t, \theta_0, \eta_0), \eta(t, \theta_0, \eta_0))$ is the solution of system (4.1) initiated from (θ_0, η_0) at $t = 0$. We iterate Π from points near the saddle $A_- : (-\pi, 0)$ and the heteroclinic orbit Γ_+, while we iterate the inverse Π^{-1} from points near the saddle $A_+ : (\pi, 0)$ and the heteroclinic orbit Γ_+. Then we separately simulate orbits under the Poincaré map near the unstable manifold of A_- and near the stable manifold of A_+. To illustrate our results, we prefer the value $K = 10$ rather than a larger $K = 10,000$ for the limited capacity of our Pentium IV computer. The following figures are plotted with MATLAB 6.5 software. Figures 5, 6, and 7 show
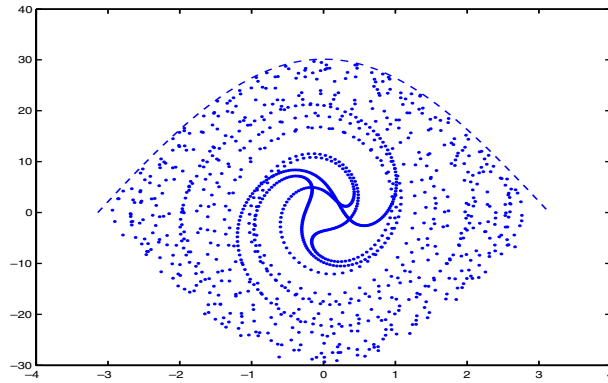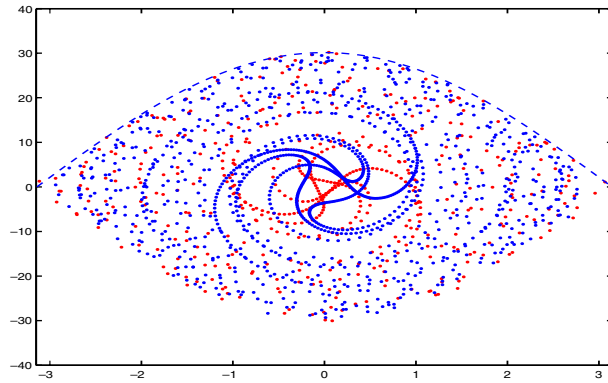
FIG. 7. $\Xi = 0.02$ and $\Lambda = 0.04$.
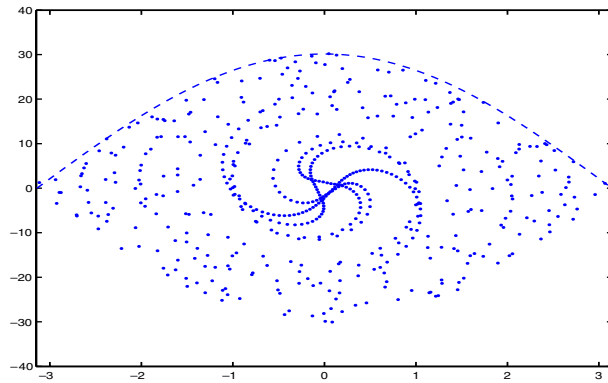
FIG. 8. $\Xi = 0.02$ and $\Lambda = 0.04$.

the orbits near the unstable manifold, and Figure 8 shows the orbit near the stable manifold, where the dashed curve is the heteroclinic orbit Γ_+ of the unperturbed system (3.1). Figure 9 shows the orbits near the unstable manifold blended with the orbits near the stable manifold for $(\Xi, \Lambda) = (0.02, 0.04)$, which obviously lies in the region $\mathcal{K}^2_{\varepsilon,\varepsilon'} = \{(\Xi, \Lambda) \in \mathbf{R}^2 : |\frac{\Lambda}{\Xi}| > 1.9449\}$ for $K = 10$. In Figure 9 the phenomenon of transversal intersection between the simulated stable manifold and unstable manifold is obvious, which displays the character of the Smale horseshoe.

6. Conclusion. In this paper we deal with a problem often encountered in practice: how to use Melnikov's method to analyze chaotic behavior of a nonlinear system whose homoclinic (or heteroclinic) orbits cannot be solved analytically.

First, based on geometric analysis, a rigid shaft of rotor on a low-speed balance platform is modeled. This model includes a complicated nonlinear function that brings difficulties in investigating the distribution and qualitative properties of its equilibria. Further, the nonlinearity also makes it difficult to obtain closed forms for heteroclinic orbits, which must be used when computing Melnikov functions.

By applying this nonlinear model as an illustrative example, a numerical algorithm is then given to compute Melnikov functions. In the algorithm, we use appropriate numerical approximation rules and techniques such as estimating modulus of continuity and reduction to infinite sums to deal with infinite integrating intervals, infinitely

FIG. 9. $\Xi = 0.02$ and $\Lambda = 0.04$.

oscillatory integrands, and low-order continuity of integrands. A series of approximation error analysis is carried out to estimate and control the numerical precision.

Following this algorithm we can determine the region of parameters with arbitrary precision wherein the nonlinear model with damping and periodic external excitation behaves chaotically. Finally, the effectiveness of this algorithm is demonstrated through a number of simulations on the nonlinear rotor system.

REFERENCES

[1] P. ASHWIN AND Z. MEI, *A numerical bifurcation function for homoclinic orbits*, SIAM J. Numer. Anal., 35 (1998), pp. 2055–2069.

[2] J.H. CHEN, K.T. CHAU, C.C. CHAN, AND Q. JIANG, *Subharmonics and chaos in switched reluctance motor drives*, IEEE Trans. Energy Conversion, 17 (2002), pp. 73–78.

[3] D. CHILDS, *Turbomachinery Rotordynamics*, John Wiley & Sons, New York, 1993.

[4] K. CZOLCZYNSKI, *Rotordynamics of Gas-Lubricated Journal Bearing Systems*, Springer-Verlag, New York, 1999.

[5] P.J. DAVIS AND P. RABINOWITZ, *Methods of Numerical Integration*, Academic Press, New York, 1975.

[6] T.O. ESPELID AND K.J. OVERHOLT, *DQAINF: An algorithm for automatic integration of infinite oscillating tails*, Numer. Algorithms, 8 (1994), pp. 83–101.

[7] L. FIELDING, *Turbine Design: The Effect on Axial Flow Turbine Performance of Parameter Variation*, ASME Press, New York, 2000.

[8] M.J. GOODWIN, *Dynamics of Rotor-Bearing Systems*, Unwin Hyman, London, 1989.

[9] W. GOVAERTS, YU. A. KUZNETSOV, AND B. SIJNAVE, *Numerical methods for the generalized Hopf bifurcation*, SIAM J. Numer. Anal., 38 (2000), pp. 329–346.

[10] G.L. GRAY, I. DOBSON, AND D.C. KAMMER, *Chaos in a spacecraft attitude manoeuvre due to time-periodic perturbations*, Trans. ASME J. Appl. Mech., 21 (1996), pp. 501–508.

[11] J. GUCKENHEIMER AND P. HOLMES, *Nonlinear Oscillations: Dynamical Systems and Bifurcations of Vector Fields*, Springer-Verlag, New York, 1983.

[12] J. GUCKENHEIMER, M. MYERS, AND B. STURMFELS, *Computing Hopf bifurcations* I, SIAM J. Numer. Anal., 34 (1997), pp. 1–21.

[13] J. GUCKENHEIMER AND B. MELOON, *Computing periodic orbits and their bifurcations with automatic differentiation*, SIAM J. Sci. Comput., 22 (2000), pp. 951–985.

[14] J.K. HALE, *Ordinary Differential Equations*, Wiley-Interscience, New York, 1969.

[15] P.J. HOLMES, *A nonlinear oscillator with a strange attractor*, Philos. Trans. Roy. Soc. London Ser. A, 292 (1979), pp. 419–448.

[16] P.J. HOLMES AND J.E. MARSDEN, *Horseshoes in perturbations of Hamiltonian systems with two degrees of freedom*, Comm. Math. Phys., 82 (1981/82), pp. 523–544.

[17] D. JACKSON, *The Theory of Approximation*, AMS, New York, 1930.

[18] C.-S. KIM AND C.-W. LEE, *Isotropic control of rotor bearing system*, in Vibration of Rotating Systems, K.W. Wang and D. Segalman, eds., ASME, New York, 1993, pp. 325–329.

[19] J. KUANG, S. TAN, AND A.Y.T. LEUNG, *On Melnikov's method in the study of chaotic motions of gyrostat*, Internat. J. Control, 75 (2002), pp. 328–351.

[20] L. LIU, G. MOORE, AND R.D. RUSSELL, *Computation and continuation of homoclinic and heteroclinic orbits with arclength parameterization*, SIAM J. Sci. Comput., 18 (1997), pp. 69–93.

[21] J.N. LYNESS, *Integrating some infinite oscillating tails*, J. Comput. Appl. Math., 12/13 (1985), pp. 109–117.

[22] J.H. PENG AND Y.Z. LIU, *Chaotic motion of a gyrostat with asymmetric rotor*, Internat. J. Non-Linear Mech., 35 (2000), pp. 431–437.

[23] T. SAUTER, *Computation of irregularly oscillating integrals*, Appl. Numer. Math., 35 (2000), pp. 245–264.

[24] A. SIDI, *Extrapolation methods for oscillatory infinite integrals*, J. Inst. Math. Appl., 26 (1980), pp. 1–20.

[25] X. TONG, B. TABARROK, AND F.P.J. RIMROTT, *Chaotic motion of an asymmetric gyrostat in the gravitational field*, Internat. J. Non-Linear Mech., 30 (1995), pp. 191–203.

[26] W. ZHANG AND W.D. ZHANG, *Chaotic oscillation of a nonlinear power system*, Appl. Math. Mech., 20 (1999), pp. 1175–1182.

[27] S. ZHOU AND J. SHI, *Imbalance estimation for speed-varying rigid rotors using time-varying observer*, J. Dyn. Syst. Meas. Contr., 123 (2001), pp. 637–644.